

We are IntechOpen, the world's leading publisher of Open Access books Built by scientists, for scientists

4,800

Open access books available

122,000

International authors and editors

135M

Downloads

Our authors are among the

154

Countries delivered to

TOP 1%

most cited scientists

12.2%

Contributors from top 500 universities



WEB OF SCIENCE™

Selection of our books indexed in the Book Citation Index
in Web of Science™ Core Collection (BKCI)

Interested in publishing with us?
Contact book.department@intechopen.com

Numbers displayed above are based on latest data collected.
For more information visit www.intechopen.com



Open Acoustic Barriers: A New Attenuation Mechanism

Constanza Rubio, Sergio Castiñeira-Ibáñez,
Juan Vicente Sánchez-Pérez, Pilar Candelas,
Francisco Belmar and Antonio Uris

Additional information is available at the end of the chapter

<http://dx.doi.org/10.5772/64360>

Abstract

One of the main environmental problems of the industrialised countries is the noise, which can be defined as an unwanted or unpleasant outdoor sound generated by transport, industry and human activities in general. When it is not possible to reduce the emission of noise acting on the source, the reduction of noise levels in its transmission phase using acoustic screens (AS) seems appropriate; such screens are in common use to reduce noise levels and have been extensively studied since the middle of the 20th century. Over the last decades, various acoustic screen designs have been investigated to increase the screening effect. The research carried out focuses on both the reduction of diffraction at the top edge of the screen by varying the shape at the top or adding absorptive materials to the noise screen, but all these screens are basically formed by a continuum rigid material with a superficial density high enough, to reduce transmission of noise through the screen, in accordance with the mass law. At the end of the nineties, another type of screen based on arrangements of isolated scatterers embedded in air, emerged. Among other interesting properties, these screens provide new mechanisms to control the noise based on the Bragg law. First, a Sonic Crystal Acoustic Screen (SCAS) was presented, where the scatterers are arranged following crystalline patterns. After that, a new prototype of AS based on sonic crystals appears, which increases the attenuation capabilities using arrangements based on fractal geometries. The screens designed in this way have been referred to as Fractal-based Sonic Crystal Acoustic Screens (FSCAS) in this chapter. In both the cases, the mechanism that prevents the transmission of noise, and therefore increases the noise attenuation, is the destructive Bragg interference due to a multiple scattering process. Finally, a new concept of AS based on a periodic arrangement of scatterers, with a slit dimension between them that is smaller than the wavelength is introduced. This latest screen is called Subwavelength Slit Acoustic Screen (SSAS) which presents a Wood anomaly and Fabry-Perot resonances, being the destructive interferences among the scattered waves, responsible for the attenuation capabilities of these screens. This new kind of AS (SCAS, FSCAS and SSAS) presents interesting properties and can be considered as a real

alternative to the classical AS, which are formed by a continuum rigid material. The aim of this chapter is to present these open AS, and it is organised as follows. In Section 1, an introduction about classic acoustic screens is presented. Numerical models and experimental set-up for the screens are introduced in Section 2. Then, in Section 3 the transmission properties of Sonic Crystals are explained, and the research advances in this field related to the design of a screen based on the new mechanism of noise control are highlighted. The definition and development of the Fractal-based Sonic Crystal Acoustic Screen are shown subsequently. The Subwavelength Slit Acoustic Screen is developed in Section 4. Finally, in Section 5 the main results and conclusions of the work are presented.

Keywords: acoustic barrier, sonic crystal, subwavelength slit, acoustic attenuation, insertion loss

1. Introduction

Noise pollution is an important environmental problem of the twenty-first century society that affects millions of people around the world. In urban areas where noise pollution is due to different noise sources, such as traffic noise, industrial noise and many other noise sources, the citizens are exposed to high noise levels, which have been linked to various health problems such as fatigue, sleep disturbance, cardiovascular disorders and/or some reduction on performance at work or school [1, 2]. In general, noise travels from the source to the receiver in a straight line, so that we can act on both the source (reducing noise generated by motors and machinery, for example) on the receiver (installing more insulation enclosures such as double windows) or on the noise transmission phase (installing acoustic screens) to control the noise that reaches the receiver [3]. When it is not possible to reduce the emission of the noise acting on the source or on the receiver – technically or economically – the most effective and common method to reduce the noise levels is the use of acoustic screens (AS). A classical AS is defined as any relatively opaque solid to sound that blocks the line of sight from the sound source to the receiver. In order to satisfy this, screens have to be made with continuum rigid materials (without openings) since the procedure which reduces sound transmission is the mass law, as discussed above, the superficial density must be at least 20 kg/m^2 . The acoustic mechanism involved in this kind of screen is simple: The interposed object (the screen) reduces the noise levels that reach the receiver through diverse mechanisms such as absorption, reflection or diffraction (see **Figure 1**). This latest mechanism means that the acoustic wave, rather than following the direct path, it is forced to spread over or around the screen. This mechanism can be considered as one of the main factors that decreases the effectiveness of the screens [4]. The zone where sound waves do not arrive through the straight path is called the shadow zone. Here the sound pressure level is mainly due to diffraction.

Many researchers [5–9] have studied the performance of AS with different top patterns. Apart from this research line, uninteresting advances in this research file have been obtained, leading to a stagnation in the technological development in the field of AS.

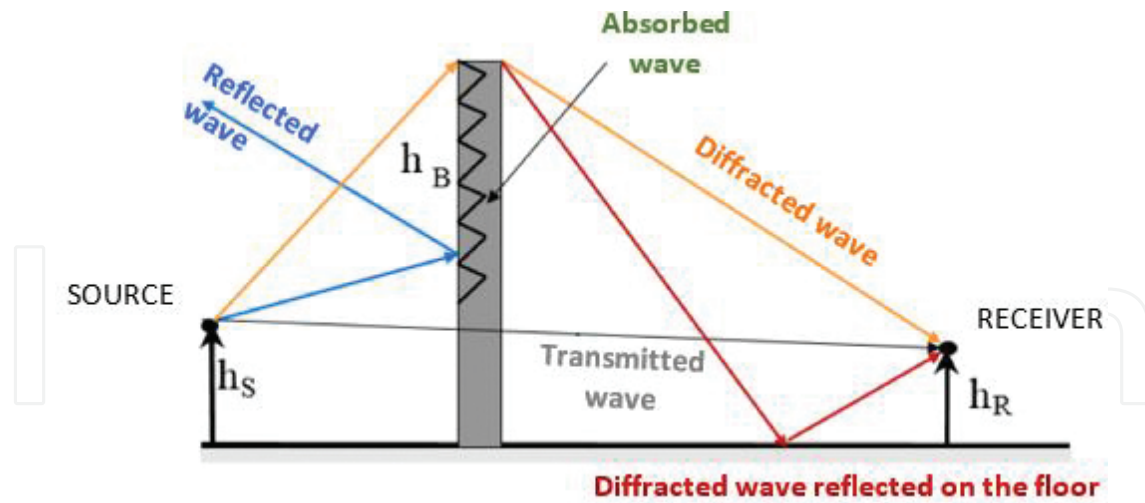


Figure 1. Noise path and acoustic behaviour of sound when an acoustic screen is placed between source and receiver.

At the end of the nineties, a new research line focused on alternative screen systems has received considerable attention. This chapter reports the modelling, development and testing of this new kind of screens that includes another physical mechanism to control the transmission of acoustic waves. Non-acoustic factors such as cost, practical and engineering issues, aesthetic or environmental impacts must be taken. The need for an AS may be mostly driven by acoustic concerns; however, non-acoustic factors are as important as the acoustic ones in the final design and construction.

Finally, it must be pointed out that the index commonly used to express the acoustic attenuation obtained by installing AS is the insertion loss (IL). This index is defined as the difference between the sound pressure levels recorded at the same point with and without the screen. Throughout this chapter, IL will be used to standardise and compare the acoustic behaviour of the different devices presented.

2. Numerical model and experimental results

The development of theoretical models that explain the interaction of acoustic waves with different objects is one of the fundamental pillars in the development of acoustics, allowing us to understand both the underlying physics in new systems and devices, as well as studying their potential technological applications. In order to predict the performance of an AS before fabrication, numerical calculations have been made. Due to the characteristics of the devices analysed, the Finite Element Method (FEM) seems a good theoretical tool to design this kind of noise screen. Thus, a commercial software Comsol Multiphysics 3.5a, Acoustics Pressure Module (Time Harmonic Analysis) is used for modelling the different screens proposed. A free and fine mesh parameter, with the regular refinement method was selected.

The wave equation, partial differential equation (PDE), is given by the expression [10]:

$$\nabla \left(\frac{1}{\rho_0} \nabla p \right) + \frac{\omega^2}{c^2 \rho_0} p = 0$$

In order to analyse the behaviour of the screen a plane wave impinging on it is considered. Throughout this chapter, and for all the new screens defined, we only consider the normal incidence of the wave on the structure. This plane wave can be expressed as follows:

$$p_{in} = e^{j\omega x}$$

The noise attenuation spectrum, at a point behind the sample, is obtained for the different cases. To do that, the difference between the direct and interfered sound pressure evaluated by means the Insertion Loss (IL) parameter at that point, has been calculated as follows:

$$IL = 20 \cdot \log_{10} \left| \frac{P_{direct}}{P_{Interfered}} \right|$$

Concerning boundary conditions used in this model, it is had [10]:

- *Sound-Hard Boundary (Wall)*: This is a boundary condition of the Neumann type, implying that the partial derivative of the pressure at the surface is zero. This means that the amplitude of the pressure at this surface will be maximum or minimum.
- *Radiation Boundary Condition*: It allows the wave travelling out the modelling domain, with minimal or no reflection, that is, the scattered field consists only of outgoing waves. This condition is also called the Sommerfeld condition.
- *Perfectly Matched Layers (PML)*: in situations where it is not possible to describe in a simple way, the outgoing radiation with a known wavenumber and its propagation direction, PMLs offer a powerful alternative: while a PML has the same function, it is not a boundary condition but an additional domain that absorbs the incident radiation without producing reflections. PML provides good performance for a wide range of angles of incidence being insensitive to the shape of the wave fronts. PML therefore is able to emulate the limits avoiding reflections.

The height of the scatterers for all the screens defined is considered infinite, so the diffraction at the top edge was not considered and the structure can be considered by means of a two dimensional (2D) model.

By a way of example, in **Figure 2**, these conditions and the possibility to obtain pressure maps and the attenuation spectrum are shown. The structure, which is placed in the numerical domain, will be any of the screens shown afterwards such as SCAS, FSCAS or SSAS, because all of them can be considered formed by rigid scatterers.

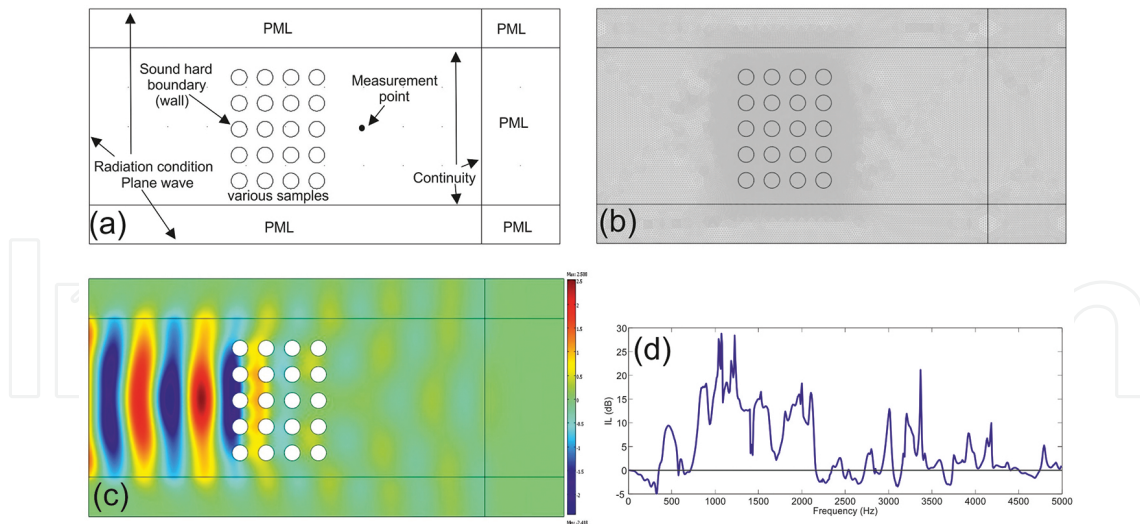


Figure 2. (a) Main conditions of the numerical solution domain. (b) Numerical domain mesh of 2.5×10^5 elements. (c) Numerical simulation of the scattering problem at 1000 Hz. The real value of the total pressure, $\text{Re}(P)$, is plotted. (d) Attenuation spectrum at a selected point.

To validate the numerical results obtained by means of our model, a set of experiments have been performed in an echo-free chamber of size $8 \times 6 \times 3 \text{ m}^3$, which simulate free field conditions [11]. A prepolarized free-field 1/2" microphone Type 4189 B&K located at 1 m from the sample and a directional sound source GENELEC 8040A emitting continuous white noise, located 1 m behind the sample in order to consider the wave impinging on the sample as a plane wave, have been used throughout the experiments. The position of the microphone is controlled and varied by using a Cartesian robot, which we have called the three-dimensional Robotized e-Acoustic Measurement System (3DReAMS), which is capable of sweeping the microphone through a 3D grid of measuring points located at any trajectory inside the chamber. When the robotized system is turned off, the microphone acquires the temporal signal. This signal is saved on the computer and then the frequency response of the measured sample is obtained using the Fast Fourier Transform (FFT). For both the data acquisition and the motion of the robot, the National Instruments cards PCI-4474 and PCI-7334 have been used together with the Sound and Vibration Toolkit and the Order Analysis Toolkit for LabVIEW. The sample was hanging from a frame in such a way that there was no influence of ground effect. Experimental results shown in this chapter have been obtained, basically, by means of this experimental set-up. The special features will be commented in sections 3 and 4.

3. Sonic Crystal Acoustic Screen (SCAS)

3.1. Main characteristics on sonic crystals

The first option presented as an alternative to classical acoustic screens is the use of sonic crystals (SCs). A SC can be defined as a heterogeneous material consisting of a periodic array of acoustic scatterers embedded in a medium with different physical properties, where one of

the materials is a fluid [12]. Depending on the number of directions where the periodicity of the array exists, one, two or three-dimensional SCs can be defined (see **Figure 3**). The mechanism that forbids the sound transmission through the system is different from those that prevail in classical AS, in this case the underlying physical mechanism is the destructive Bragg interference due to a Multiple Scattering (MS) process [13], related to the periodicity of the system. These destructive interferences lead to attenuation peaks. These peaks widen with an increase of both the number and the diameter of the cylinders, thus these periodic systems exhibit ranges of frequencies related to the periodicity of the structure where there is no wave propagation. These ranges of frequency are called Band Gaps (BGs). Other physical mechanisms such as absorption or reflection can be added to the scatterers increasing the attenuation capabilities.

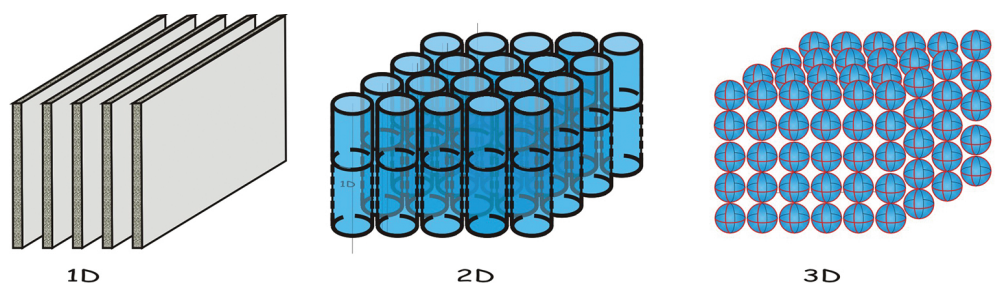


Figure 3. One, two and three-dimensional Sonic Crystal.

The use of SCs as AS implies that the scatterers are formed by rigid materials and the fluid medium is air. Furthermore, although the shape of the scatterers is related to the attenuation properties of these systems [14], the most used in the two-dimensional case is the cylindrical shape, mainly due to the ease of calculation associated with its geometry because of its symmetry properties. Therefore, we will consider two-dimensional sonic crystals (2DSC) formed by cylindrical scatterers with variable height and radius, and the screens formed in this way are called Sonic Crystal Acoustic Screens (SCAS).

Regardless of the shape, the scattering of the incident wave in each and every one of the scatterers of the SC leads to the existence of the BGs. The existence of the BGs is one of the most interesting properties of SCs and it is the responsible for their use as AS.

Both the position and the size of these BG depend, in the frequency domain, on several factors [15] such as: (i) the spatial distribution of the scatterers; (ii) the separation between the scatterers; (iii) the densities and the contrast of propagation velocities between the air and the scatterers and (iv) The amount of mass of the scatterers per unit area of the crystalline array. Next, the influence of these factors on the existence of the band gaps is briefly explained.

- i. **Spatial distribution of scatterers.** This factor indicates how the scatterers are arranged in the crystal. Thus, for instance, if the chosen symmetry is triangular, scatterers are located at the vertices of the triangle; if the symmetry is square, at the corners of squares, and so on. The most suitable crystalline symmetries for 2DSC screens are square and triangular lattices.

- ii. Separation between scatterers. This factor is given by the lattice constant and indicates the size of the triangles, squares, etc., which form the array under consideration. It is closely related to the previous factor because if the spatial distribution of scatterers defines how they are distributed; the lattice constant determines how much these scatterers are separated from one another. Furthermore, it is crucial in such a periodic system because it defines the relationship between the geometrical properties of the lattice and the position of the attenuation band in such a way that when the separation decreases, the position of the attenuation band in the frequency domain increases and vice versa. Therefore, by increasing the lattice constant very low frequencies could be attenuated.
- iii. The densities and the contrast of propagation velocities between the air and the scatterers determine the size of the BGs and their position in the frequency domain. In our case, the material that forms the scatterers must be acoustically rigid; with its propagation velocity and its density values being much higher than those of air. This fact allows the use of almost any material in the design of the scatterers.
- iv. The amount of mass of the scatterer per unit area of the crystalline array. This relationship is given by the filling fraction, which represents the relation between the area occupied by scatterers and the area of the lattice. In general, the higher the filling fraction the broader the BG (see **Figure 4**).

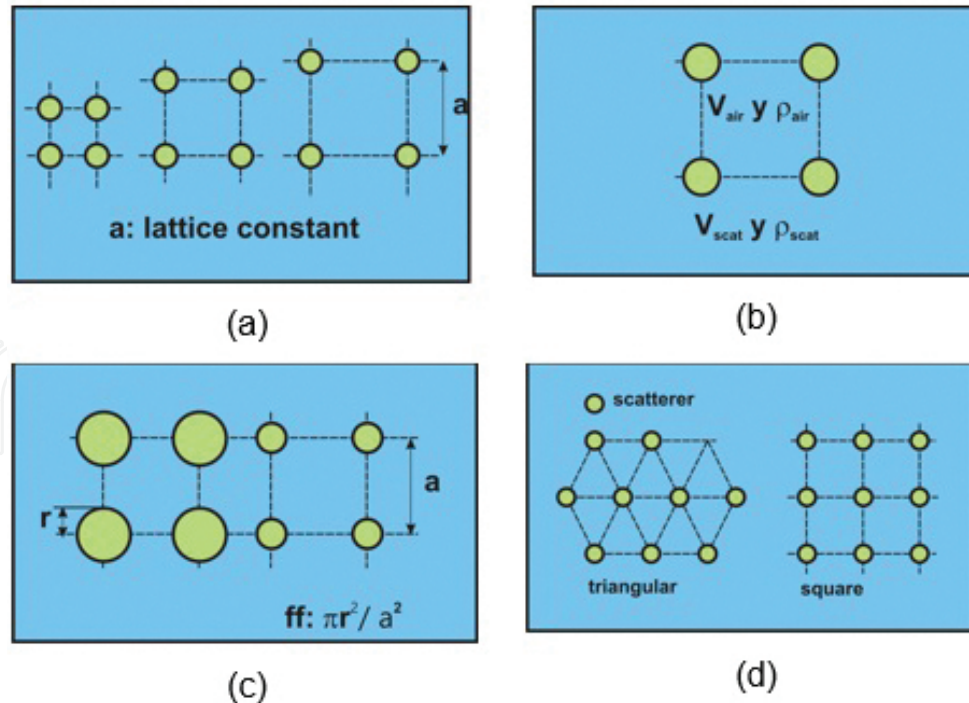


Figure 4. Main parameters that determine both the position and the size of the BGs. (a) Separation between scatterers (lattice constant). (b) The densities and the contrast of propagation velocities between the air and the scatterers. (c) The amount of mass of the scatterers per unit area of the crystalline array (ff). (d) Spatial distribution of scatterers.

Moreover, the position of the BG in the frequency domain depends on the direction of incidence of the acoustic wave on the SC.

Another parameter commonly used to quantify the noise attenuation in a range of frequencies is the attenuation area (AA), defined as the area enclosed between the positive attenuation spectra and the 0 dB threshold in the frequency range selected [16].

Symmetry	Bragg's frequency	Filling fraction
Square	$f_{\text{Bragg}} = \frac{c}{2a}$	$ff_{\text{square}} = \frac{\pi r^2}{a^2}$
Triangular	$f_{\text{Bragg}} = \frac{c}{\sqrt{3}a}$	$ff_{\text{triangular}} = \frac{2\pi r^2}{\sqrt{3}a^2}$

Table 1. Mathematical expressions for determining the Bragg's frequency and filling fraction for square and triangular symmetries. Cylindrical scatterers are considered as having r for its radii and a is the lattice constant.

Where the scatterers are cylindrical and sound impinges perpendicularly onto the screen, the Bragg frequencies and the filling fraction for square and triangular symmetry are those summarised in **Table 1**.

In **Figure 5a**, the attenuation spectrum of a SC formed by 60 cylindrical scatterers with radii $r = 0.09$ m arranged in a square lattice with lattice constant $a = 0.22$ m is represented. With these characteristics, the Bragg frequency of the attenuation peak is given as follows:

$$f_{\text{Bragg}} = \frac{c}{2a} = 772 \text{ Hz}$$

The frequencies where the wavelength is approximately twice the lattice constant, form part of the first BG. In this figure, the first and the second BGs can be observed. In **Figure 5b**, the attenuation spectrum of a SC formed by 60 cylindrical scatterers with radii $r = 0.02$ m arranged in a triangular lattice with lattice constant $a = 0.0635$ cm is represented. In this case, the Bragg frequency is given as follows:

$$f_{\text{Bragg}} = \frac{c}{\sqrt{3}a} = 2677 \text{ Hz}$$

In both the cases SCs are formed by 6 rows each of 10 cylinders each one, with the incident wave (IPW) being normal to the structure.

As it noted above, the position of the BG in the frequency domain depends on the direction of incidence of the acoustic wave on the SC. However, if wide BGs are achieved an overlap between bands for different orientations can exist. In the overlap area, the screen attenuates

regardless of the direction of incidence. In summary, the distance between the scatterers and the angle of incidence of the wave on the sonic crystal determines the central frequency of the BG, and the section size of the scatterers determines the width of frequencies of the attenuation bands. Throughout this chapter the incidence is considered normal to the structure.

It is worth noting that with the Bragg interference being the only mechanism to control the sound attenuation it is difficult to ensure a good design and construction of an efficient acoustic screen based on sonic crystals. To avoid this problem and also improve the attenuation properties of the SCAS, two research lines have been followed. On one hand, to avoid the dependence with the angle of incidence of the acoustic wave on the structure and, on the other, to maximise the destructive interference. For the first one, additional physical properties have been introduced to the scatterers such as absorption and resonances [17]. For the second one, novel arrangements of scatterers which are different from the crystalline symmetries that allow the overlapping of acoustic bands have been sought. This second research line is further developed in this chapter.

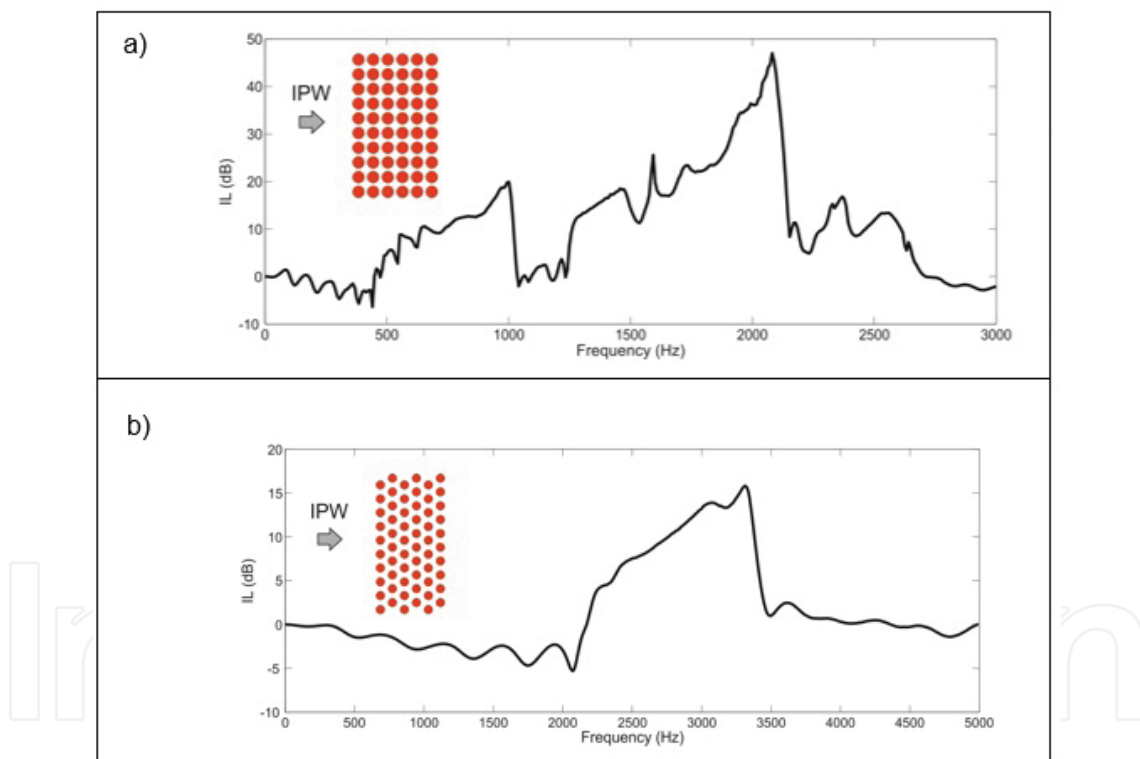


Figure 5. Attenuation spectra for normal incidence. (a) Square lattice, lattice constant $a=22$ cm and cylinder radii $r=9$ cm is represented. (b) Triangular lattice, lattice constant $a=6.35$ cm and cylinder radii $r=2$ cm.

3.2. Fractal-based Sonic Crystal Acoustic Screen

In nature there are objects whose structure has the property of scale invariance, that is, the whole seems geometrically equal to the parts. The objects that contain copies of themselves within them are usually called fractals. Fractal geometries have been applied in several

sciences, such as medicine, biology [18] or economics [19]. In the case of SC, fractals have been traditionally used to design the shape of the scatterers [20] or to reallocate the total mass of the scatterers in a predetermined device [21].

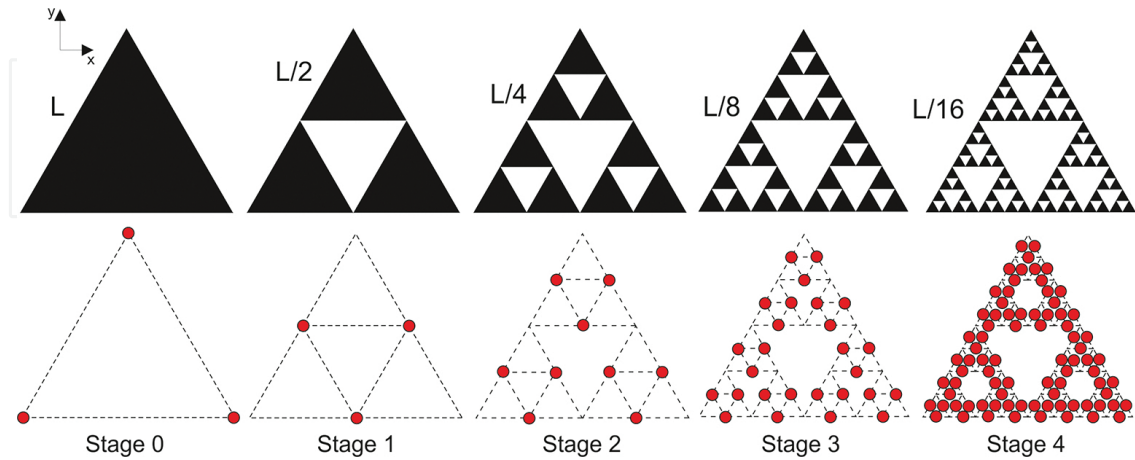


Figure 6. Quasi-fractal arrangement of scatterers: Five stages of cylinder arrays based on Sierpinski's triangle geometry.

This section provides a procedure based on the redistribution of the mass of the scatterers of SC following fractal geometries in order to increase the attenuation bands obtained by Bragg diffraction [21].

For this purpose, a well-known fractal called the Sierpinski triangle, whose formation can be seen at the top of **Figure 6**, has been used to design a two dimensional structure of isolated rigid cylinders with a high attenuation performance. As can be seen at the bottom of **Figure 6** the new arrangement of the scatterers is formed by placing them following this fractal geometry. Bearing in mind that fractal construction results from an infinite iterative process, that is, it results from the repetition of an identical theme at different size scales [22], the structure showed in **Figure 6** is called Quasi-Fractal Structure (QFS) due to the fact that only the first five stages or iterations are shown [21].

Moreover, QFS could be considered as classic triangular arrangements in which some cylinders have been removed, creating some vacancies in the array. However, the underlying symmetry follows a fractal pattern. Therefore, QFS can be considered as a sum of several triangular arrays with a different lattice constant (Remember that the lattice constant has been introduced in Section 2 and it is the distance between scatterers), such as L , $L/2$, $L/4$, $L/8$ and $L/16$ as shown in **Figure 6**, corresponding to each fractal stage. This procedure provides small and compact devices where the whole attenuation band obtained can be considered as the sum of the BG of each triangular array that forms the QFS.

In **Figure 7**, a cross section of the new arrangement is shown (in the plane OXY), considering cylinders of radius r parallel to the Z-axis. Although QFS could be considered as a classical triangular array with the same vacancies, one has to take into account that the underlying growth is fractal.

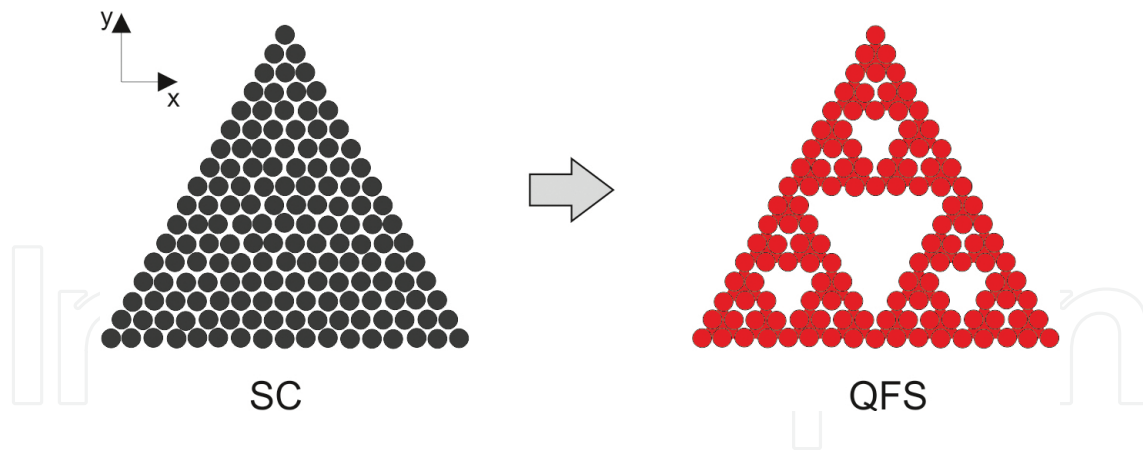


Figure 7. Starting SC and resulting QFS structures.

With this process, a compact device has been obtained. Then as a second step, in order to maximise the BG based on the quasi-fractal arrangement obtained, the radii of the scatterers have been varied at each stage. Bearing in mind that the efficiency of the ff is what is being searching, biggest radii were chosen for stage 1 and then, as the stage increases, the radius decreases. According to this second step, the most important features of this design technique will be explained right after.

For this maximisation process, the golden proportion was used to design the radii of the cylindrical scatterers. In **Figure 8**, the quasi-fractal proposed QFS_{Max} which were constructed in accordance with the golden proportion among the radii of the cylinders of stages s ($s = 0, 1, 2, 3, 4$) is shown. The radius at each stage is listed in **Table 2**.

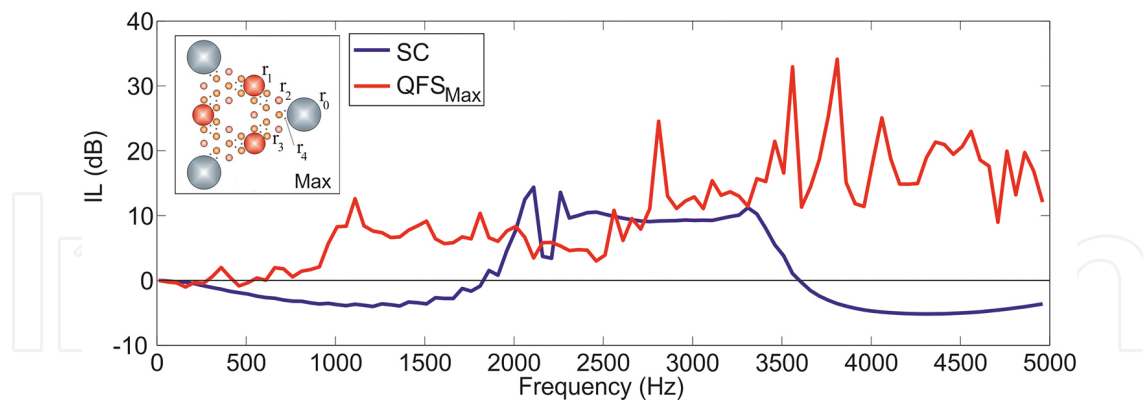


Figure 8. Sound attenuation spectra (IL) at normal incidence for both the starting SC and QFS_{Max} . In the inset, one can see a section of the quasi-fractal designed.

r_0	r_1	r_2	r_3	r_4
14.8 cm	9 cm	5.6 cm	3 cm	1.9 cm

Table 2. Theoretical radii of the of the cylinders of stages s (r_i) following the golden proportion.

It should be noted that it was necessary to remove some of the cylinders of the starting QFS shown in **Figure 8**, in order to place the larger cylinders (larger radius) of the, first iterations. It is worth noting that for other applications, the relationships between the radii of the cylinders could vary.

Comparing the values of the AA parameter for QFS_{Max} and a SC with similar size and external shape, made of rigid cylinders (radius, $r = 2$ cm) and arranged in a triangular lattice ($a = 6.35$ cm), interesting results can be observed: the value of the AA parameter for QFS_{Max} ($AA_{Max} = 51048$ Hz·dB) grows by over 340% compared to the starting SC ($AA_{SC} = 14705$ Hz·dB).

To build the QFS_{Max} it is necessary to adapt to the sizes of commercial scatterers. With this in mind, a QFS_{Exp} has been constructed with the available cylinders, with the radii in this case being listed in **Table 3**.

r_0	r_1	r_2	r_3	r_4
10	8	5.5	3	1.75

Table 3. Commercial radii of the of the cylinders of stages s (r_i) for QFS_{Exp} .

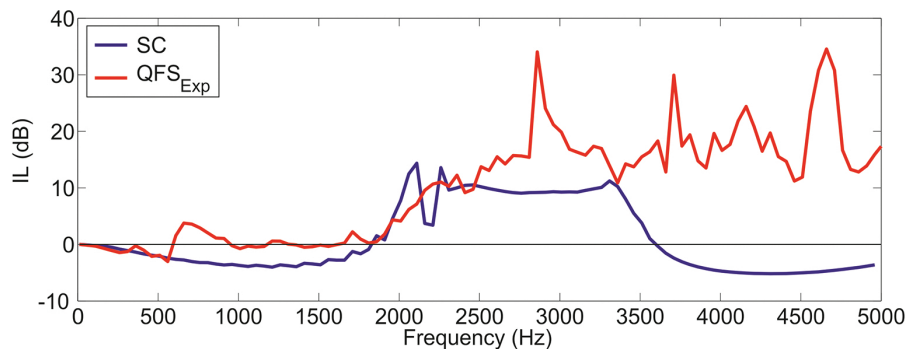


Figure 9. Spectrum sound attenuation (IL) at normal incidence to the starting SC and QFS_{Exp} .

Figure 9 shows the IL spectra for the case of commercial scatterers QFS_{Exp} and the starting SC, obtaining very interesting numerical results.

Thus, by comparing the values of the AA parameter for QFS_{Exp} ($AA_{Exp} = 42391$ Hz·dB) and the starting SC ($AA_{SC} = 14705$ Hz·dB), by over than 280% of enhancement is obtained for the QFS_{Exp} .

Table 4 summarises the results:

Sample	No. of scatterers	ff (%)	AA (Hz·dB)
SC	136	36	14,705
QFS_{Max}	60	45.8	51,048
QFS_{Exp}	60	33.24	42,391

Table 4. Number of scatterers, filling fraction (ff) and attenuation area (AA) for SC, QFS_{Max} and QFS_{Exp} .

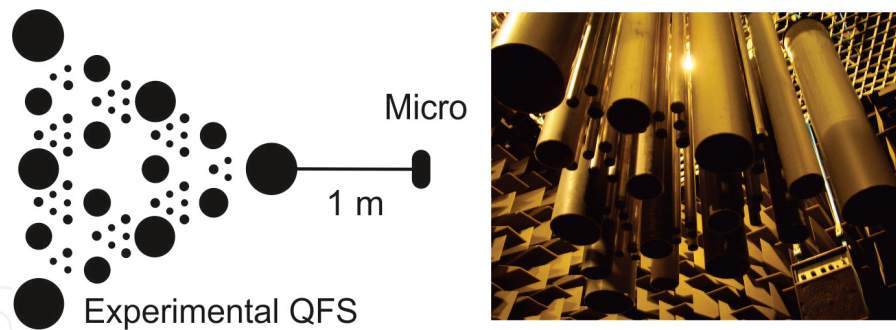


Figure 10. QFS experimental and QFS structure picture, taken from below the structure in an anechoic chamber.

With these results, the rule of the bigger ff the bigger BG size is broken. QFS produces wider BG band even though the ff decreases comparing the values with respect to the starting SC.

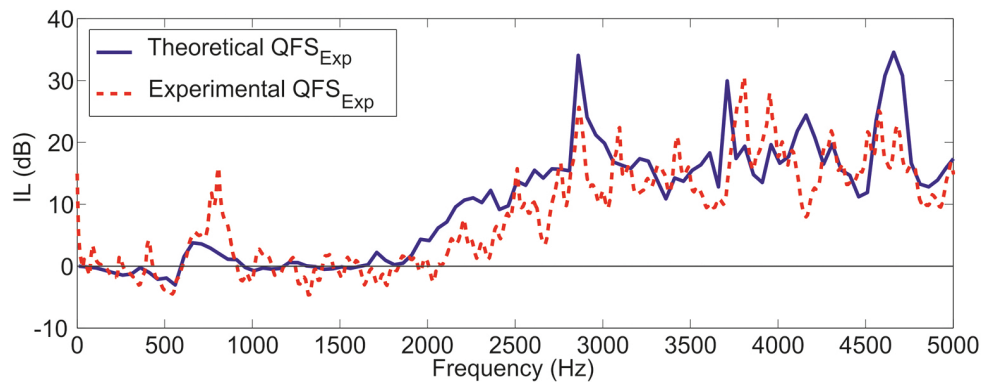


Figure 11. QFS_{Exp} theoretical and experimental IL.

To demonstrate these results, experimental measurements under controlled conditions have been performed in an anechoic chamber, as explained in Section 2.

In Figure 10, the QFS structure analysed and a photograph of the same within the anechoic chamber is shown.

In Figure 11, the experimental acoustic attenuation spectrum with QFS_{Exp} having been experimentally and numerically obtained is overlapped. The close agreement between both results can be appreciated, thus validating the design carried out.

By way of conclusion, the technique developed in two steps enables us to maximize the BG at normal incidence. At the first step the scatterers are arranged according to fractal geometry and secondly, the radii of the scatterers that form this fractal structure are adjusted depending on the considered stage in order to maximize the ff at each stage.

The screens developed from the QFS_{Exp} are the FSCAS. Nowadays, there are screens designed according to this technique that have even been homologated for market placement [23].

4. Subwavelength Slit Acoustic Screen

In 1998, Ebbesen et al. [24] observed extraordinary optical transmission through metallic films perforated with subwavelength aperture arrays. Since then, this new area of study has been the subject of research. Motivated by the wave nature of electromagnetic waves and acoustic waves, the findings for optic waves were transferred to acoustics and named “extraordinary acoustic transmission” through subwavelength apertures. In 2007, Lu et al. [25] showed both theoretically and experimentally the extraordinary acoustic transmission through a 1-D grating with subwavelength slits and Hou et al. [26] reported experimentally the extraordinary acoustic transmission through a subwavelength hole array. It is accepted that the extraordinary acoustic transmission through a subwavelength aperture array is motivated by the Fabry-Perot resonances inside the apertures. In 2008, Estrada et al. [27] showed, both theoretically and experimentally, that Wood anomalies [28] were the responsible for an extraordinary shielding in perforated plates with periodic subwavelength hole arrays. The position in the spectrum of the sound attenuation peaks corresponding to the Wood anomalies depends on the lattice constant and geometry of the array. Motivated by the success of the extraordinary shielding, a new acoustic screen based on subwavelength slits had been designed as an alternative to classical acoustic and SC screens. The sound attenuation capabilities of the new screen can be tuned as a function of the geometrical parameters, as in the case of SCAS.

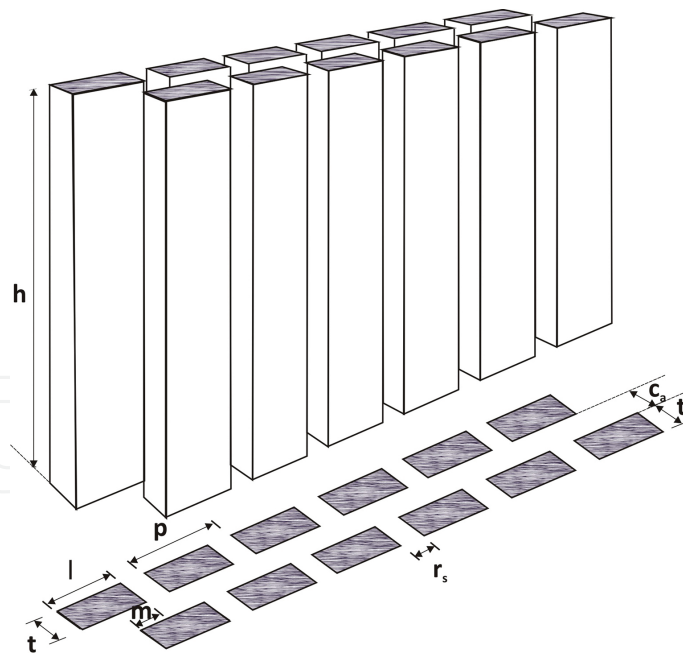


Figure 12. Schematic diagram of the subwavelength slit acoustic screen.

The basic structure considered has two rows of rigid pickets of length l and thickness t , distributed periodically with a lattice constant and with a slit width r_s . The rows are separated by an air gap c_a and the lateral misalignment between the rows is m as shown in **Figure 12**.

The effectiveness of the subwavelength-slit screen was evaluated in controlled conditions described in Section 2.

The pickets were made of wood with length $l = 0.3$ m, thickness $t = 0.1$ m and height $h = 1.8$ m, distributed periodically with a lattice constant $p = 0.35$ m, with a slit width $r_s = 0.05$ m. The rows were separated by an air gap $c_a = 0.1$ m. The picket dimensions and the periodicity were chosen to obtain the maximum attenuation corresponding to Wood anomalies at 1000 Hz.

The acoustic attenuation properties of this screen are represented by means of IL, covering a range frequency from 100 to 2500 Hz in 6 Hz steps.

In order to ensure that the position of the sound attenuation peak in the frequency domain corresponds to the Wood anomalies, several measurements for a single row of periodic array of pickets with the same characteristics as those used for the SSAS have been carried out. **Figure 13** shows the comparison between measured and calculated IL at normal incidence. Numerical computations were performed by means of FEM. The boundary conditions have been described in Section 2. The only difference with respect to **Figure 2a** is the structure that is located in the domain, in this case instead of cylinders, pickets must be placed. Pronounced insertion loss peaks can be observed, that is, the exact manifestation of the Wood anomaly [28]. The Wood anomaly for normal incidence in a periodic array of subwavelength slits is given by $\lambda = p$, where λ is the wavelength and p is the lattice period. The positions of the Wood anomalies in the frequency domain for a periodic array with $p = 0.35$ m were 971 and 1942 Hz. The Wood anomaly at the frequency of 1942 Hz is not clearly observed due to the interference with the Fabry-Perot resonance [29].

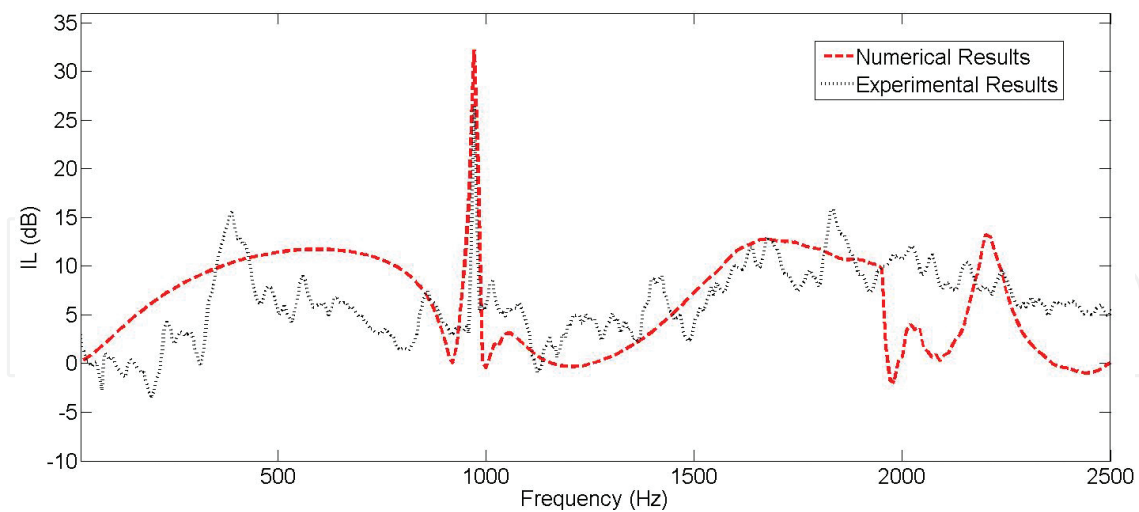


Figure 13. Calculated and measured IL at normal incidence for a single row of periodic array of pickets.

Figure 14 shows measured IL at normal incidence for the SSAS with the characteristics mentioned above. The rows were separated by an air gap $c_a = 0.1$ m. Three different values of lateral misalignment between the rows were considered $m = 0.3, 0.2$ and 0.125 m. The Wood anomaly at a frequency of 971 Hz is clearly seen. Sharp insertion loss peak at a frequency of

around 1500 Hz is also observed. This frequency corresponds to destructive interference between the odd and even Fabry-Perot modes, resulting in an IL increase.

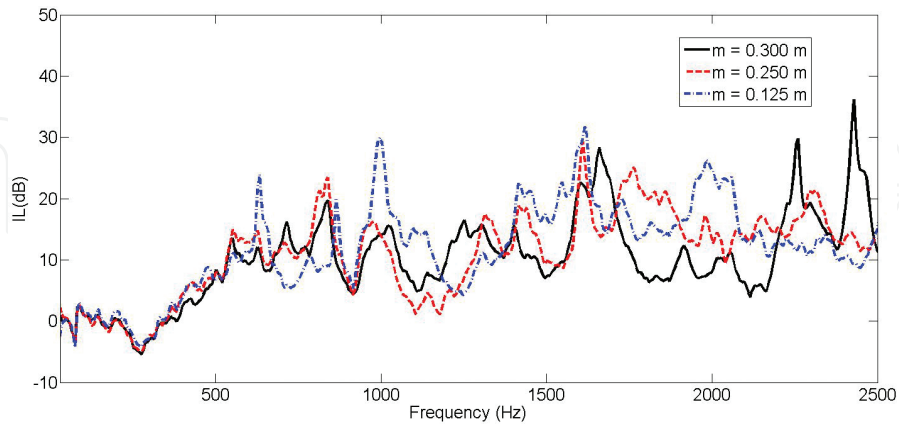


Figure 14. Measured insertion loss for an acoustic screen with two rows of pickets of length $l = 0.3$ m, thickness $t = 0.1$ m and height $h = 1.8$ m, distributed periodically with a period $p = 0.35$ m, with a slit width $r_s = 0.05$ m. The rows were separated by an air gap $c_a = 0.1$ m. Three different values of lateral misalignment between the rows were considered $m = 0.300, 0.250$ and 0.125 m.

By varying the lateral misalignment between the rows m , it is observed that, as the lateral misalignment is increased, insertion loss peaks appear at frequencies between 500 and 800 Hz which, in the case of lateral misalignment $m = 0.125$ m, did not appear. These peaks are associated with a destructive interference between the propagating and evanescent waves.

Thus, the values of the AA parameter for SSAS varying the lateral misalignment between the rows are shown in **Table 5**. With only two rows of pickets significant values of the AA parameters are achieved.

Misalignment (m)	AA (Hz·dB)
0.300	72,733
0.250	78,696
0.125	68,523

Table 5. Attenuation area (AA) for different values of lateral misalignment between the rows were considered.

5. Summary and conclusions

New types of screens based on arrangements of isolated scatterers embedded in air were presented in this chapter. First, a SCAS was presented, where the scatterers are arranged following crystalline patterns. After that, a new prototype based on sonic crystals but arranged following fractal geometries has been presented. The attenuation capabilities of these screens,

FSCAS, were enhanced by varying the filling fraction of each fractal stage separately. Finally, SSAS is introduced. Unlike the other ones, this latest screen is not based on crystalline geometry but consists of arrangements of isolated scatterers. The attenuation capabilities of these screens could be enhanced by introducing additional physical properties to the scatterers.

Author details

Constanza Rubio¹, Sergio Castiñeira-Ibáñez², Juan Vicente Sánchez-Pérez¹, Pilar Candelas¹, Francisco Belmar¹ and Antonio Uris^{1*}

*Address all correspondence to: auris@fis.upv.es

1 Physical Technologies Center, Universitat Politecnica de Valencia (Polytechnic University of Valencia), Valencia, Spain

2 Electronic Engineering Department, Universitat de Valencia (University of València), Burjassot, Valencia, Spain

References

- [1] Commission of the European Communities. Green Paper on "Future Noise Policy". Brussels: 1996. p. COM(96)540.
- [2] Burden disease from environmental noise: quantification of healthy life years lost in Europe. World Health Organization Regional Office for Europe, Copenhagen, Denmark. 2011
- [3] Harris C. M., editor. Handbook of Acoustical Measurements and Noise Control. 3rd ed. New York: McGraw-Hill; 1991.
- [4] Kotzen B., English C., editors. Environmental Noise Barriers: A Guide to Their Acoustic and Visual Design. 1st ed. London and New York: E & FN SPON; 1999.
- [5] Hothersall D.C., Crombie D.H., Chandler-Wilde S.N. The performance of T-profile and associated noise barrier. *Applied Acoustics*. 1991;32:269–281.
- [6] Okubo T., Fujiwara K. Efficiency of a noise barrier with an acoustically soft cylindrical edge for practical use. *Journal of the Acoustical Society of America*. 1999;105:3326–3334.
- [7] Watts G.R. Acoustic performance of multiple-edge noise barrier profile at motorway sites. *Applied Acoustics*. 1996; 37:44–66.
- [8] Shao W., Lee H.P., Lim S.P. Performance of noise barriers with random edge profiles. *Applied Acoustics*. 2001; 62:1157–1170.

- [9] Byung-Joo J., Hyun-Sil K., Hyun-Ju K., Jae-Seung K. Sound diffraction by a partially inclined noise barrier. *Applied Acoustics*. 2001; 62:1107–1121.
- [10] COMSOL Multiphysics User Guide: Version 3.5a, COMSOL AB, Stockholm, Sweden. 2008
- [11] Castiñeira-Ibañez, S., Rubio, C., Sánchez-Pérez, J.V. Acoustic wave diffraction at the upper edge of a two-dimensional periodic array of finite rigid cylinders. A comprehensive design model of the periodicity-based devices. *Europhysics Letters*. 2013;101:64002.
- [12] Martinez-Sala R., Sancho J., Sánchez-Pérez J.V., Gómez V., Llinares J., Meseguer F. Sound attenuation by sculpture. *Nature*. 1995; 378:241.
- [13] Chen YY., Ze Z. Theoretical analysis of acoustic stop bands in two dimensional periodic scattering array. *Physical Review E*. 2001; 64:036616.
- [14] Min R., Wu F., Zhong L., Zhong S., Liu Y.Y. Extreme acoustic band gaps obtained under high symmetry in 2D phononic crystals. *Journal of Physics D: Applied Physics*. 2006; 39:2272–2276.
- [15] Kushwaha M. Stop-bands for periodic metallic rods: Sculptures that can filter the noise. *Applied Physics Letters*. 1997; 70:3218.
- [16] Romero-García V., Fuster E., García-Raffi L.M., Sánchez-Pérez E.A., Sopena M., Llinares J., Sánchez-Pérez J.V. Band gap creation using quasicrystalline structures based on sonic crystals. *Applied Physics Letters*. 2006; 88:174104.
- [17] Romero-García V., Krynkin A., García-Raffi L.M., Umnova O., Sánchez-Pérez, J.V. Multi-resonant scatterers in sonic crystals: locally multi-resonant acoustic metamaterial. *Journal of Sound and Vibration*. 2013; 332:184–198.
- [18] Iannaccone P.M., Khokha M.. *Fractal Geometry in Biological Systems: An Analytical Approach*. CRC Press; 1996.
- [19] Willians B., Trading B.. *Chaos, Applying Expert Techniques to Maximize Your Profits*. Market place Books; 1995.
- [20] Norris R.C., Hamel J.S., Nadeau P. Phononic band gap crystals with periodic fractal inclusions: theoretical study using numerical analysis. *Journal of Applied Physics*. 2008;103:104908.
- [21] Castiñeira-Ibañez S., Romero-García V., Sánchez-Pérez J.V. García-Raffi L.M. Overlapping of acoustic bandgaps using fractal geometries. *Europhysics Letters*. 2010;92:24007.
- [22] Mandelbrot B. *The Fractal Geometry of the Nature*. New York: W.H. Freeman & Co; 1983.
- [23] Castiñeira-Ibañez S., Rubio C., Romero-García V., Sánchez-Pérez J.V., García-Raffi L.M. Design, manufacture and characterization of an acoustic barrier made of multi-

phenomena cylindrical scatterers arranged in a fractal-based geometry. *Archives of Acoustics*. 2012;37:455–462.

- [24] Ebbesen T.W., Lezec H.J., Ghaemi H.F., Thio T., Wolf P.A. Extraordinary optical transmission through sub-wavelength hole arrays. *Nature*. 1998; 391:667–669.
- [25] Lu M.H., Liu X.K., Feng L., Li J., Huang C.P., Chen Y.F., Zhu Y.Y., Zhu S.N., Ming N.B. Extraordinary acoustic transmission through a 1d grating with very narrow apertures. *Physical Review Letters*. 2007;99:174301.
- [26] Hou B., Mei J., Ke M., Wen W., Liu Z., Shi J., Sheng P. Tuning Fabry-Perot resonances via diffraction evanescent waves. *Physical Review B*. 2007; 76:054303.
- [27] Estrada H., Candelas P., Uris A., Belmar F., Garcia de Abajo F.J., Meseguer F. Extraordinary sound screening in perforated plates. *Physical Review Letters*. 2008;101:084302.
- [28] Wood R.W. Anomalous diffraction gratings. *Physical Review*. 1935; 48:928–936.
- [29] Rubio C., Candelas P., Belmar F., Gomez-Lozano V., Uris A. Subwavelength slit acoustic metamaterial barrier. *Journal of Physics D: Applied Physics*. 2015; 48:395501.

IntechOpen

IntechOpen

IntechOpen